



ESA Contract (4000144712/24/I-DT-bgh)

Contract Report to the European Space Agency

Satellite-informed fuel estimation using hybrid data assimilation

Authors: Siham El Garroussi, Francesca Di Giuseppe, Joe McNorton, Patricia de Rosnay, Sebastien Garrigues, David Fairbairn, Peter Weston Contract officer: Claudia Vitolo

November 2025

ct Report ESA Contract Re act Report ESA Contract Intract Report ESA Contract Intract Report ESA Contract Contract Report ESA Contract A Contract Report ESA Con SA Contract Report ESA A ESA Contract Report ESA SA ESA Contract Report t ESA ESA Contract Report ort ESA ESA Contract Report

ESA Contract Report ESA Contract Report ESA ESA Contract Report ESA ESA Contract Report ESA Contract Report ESA Contract Report ESA Contract Report ESA ESA Contract Report ESA CONTRACT R

Series: ECMWF ESA Contract Report Series

A full list of ECMWF Publications can be found on our web site under:

http://www.ecmwf.int/en/publications/

Contact: library@ecmwf.int

© Copyright 2025

European Centre for Medium Range Weather Forecasts, Shinfield Park, Reading, RG2 9AX, UK

Literary and scientific copyrights belong to ECMWF and are reserved in all countries. The content of this document is available for use under a Creative Commons Attribution 4.0 International Public License. See the terms at https://creativecommons.org/licenses/by/4.0/.

The information within this publication is given in good faith and considered to be true, but ECMWF accepts no liability for error or omission or for loss or damage arising from its use.



Executive summary

This deliverable presents the final outcomes of the Fuelity project, which aims to improve the representation of fuel variables in the SPARKY-fuel model through the physically constrained use of satellite information. To achieve this, we combine satellite observations with land surface modelling using a hybrid data assimilation framework implemented in the European Centre for Medium-Range Weather Forecasts (ECMWF) ecLand-integrated forecasting system (IFS).

The system ingests three complementary satellite data streams: L-band vegetation optical depth (VOD-L) -SMOS- and solar-induced fluorescence (SIF) -TROPOMI- to update a monthly leaf area index (LAI) climatology, and advanced scatterometer (ASCAT) backscatter to constrain upper-layer soil moisture. These observations are integrated using a simplified extended Kalman filter (SEKF), which updates the model background while accounting for uncertainties in both the satellite signals and the physical model, ensuring that analysis increments remain physically consistent.

Two machine-learning models, an extreme gradient boosting (XGBoost) model and a multilayer perceptron (MLP) neural network, were evaluated as observation operators to map satellite observations to their model-equivalent counterparts. The models were trained on 8-daily data over 2019–2020 to predict SIF and VOD-L from meteorological conditions, vegetation and soil states. XGBoost was retained as it provided the most effective balance of simplicity, flexibility, interpretability, and predictive skill. The operator reproduced the satellite-driven seasonal cycle with high fidelity: Validation against an independent 2021 dataset showed that LAI explained 67% of the variance in SIF and 72% in VOD-L, with corresponding RMSE values of 0.12 and 0.16 m² m⁻².

On the basis of this validation, the data assimilation framework was used to produce a 25-year global satellite-informed reanalysis of live fuel moisture content (LFMC) using the SPARKY model definition. Compared with a climatology-based LFMC benchmark, the reanalysis substantially improves the depiction of seasonal variability, drought response, and interannual fluctuations, with the greatest benefits observed in semi-arid and fire-prone ecosystems.

The system was further evaluated across three main application domains:

- Vegetation dynamics: Improved representation of phenology, drought-induced canopy decline, and fuel desiccation during major fire events.
- Fire forecasting: Earlier detection of fuel drying and improved spatial localisation of high-risk conditions, supporting the potential for near-real-time (NRT) integration into operational fire danger systems.
- Numerical weather prediction: Improved short-range forecasts of lower-tropospheric and near-surface temperatures (1000 hPa, 850 hPa, and 2 m).

These developments provide a scalable, observation-driven framework for global fuel estimation. The framework enabled the generation of satellite-constrained LFMC fields over more than 20 years. Its modular structure also creates clear pathways for future extensions to dead fuel moisture and fuel load as additional satellite missions become available, allowing progressively more complete and physically consistent fuel characterisation.



Contents

L	Data		5
	1.1	Satellite datasets	5
	1.2	Model datasets	6
		1.2.1 ECMWF land surface model - ecLand	6
		1.2.2 SPARKY	7
	1.3	Independent validation datasets	8
		1.3.1 Satellite-derived LAI observations	8
		1.3.2 ISMN in situ soil moisture observations	8
		1.3.3 MODIS active fires	8
2	Met	hodology	9
	2.1	Live fuel moisture derivation	9
	2.2	Land data assimilation framework	0
	2.3	Observation operators	13
3	Resu	ults 1	ا 4
	3.1	Observation operator performance	14
	3.2	25-year live fuel moisture reanalysis	14
	3.3	Impact evaluation	16
		3.3.1 Vegetation dynamics	16
		3.3.2 Fire forecasting	16
		3.3.3 Numerical weather prediction	18



Abbreviations

```
ASCAT
           advanced scatterometer. 1, 5, 6, 11
CDF
           cumulative distribution function. 4
CLMS
           Copernicus Land Monitoring Service. 6, 8, 9, 13,
           14, 16
DA
           data assimilation. 4, 10
ECMWF
           European Centre for Medium-Range Weather
           Forecasts. 1, 4–7
           Earth observation. 4
EO
IFS
           integrated forecasting system. 1, 5, 6, 18
ISMN
           international soil moisture network. 8, 14
LAI
           leaf area index. 1, 4–14, 16, 18–20
LFMC
           live fuel moisture content. 1, 5, 7, 9, 14, 15, 20
ML
           machine learning. 5, 13
MLP
           multilayer perceptron. 1, 13, 14
NRT
           near-real-time. 1, 18
NWP
           numerical weather prediction. 6, 10
PoF
           probability of fire. 4, 7, 16, 18
SEKF
           simplified extended Kalman filter. 1, 5
SIF
           solar-induced fluorescence. 1, 4-6, 11, 12, 14, 20
VOD-L
           L-band vegetation optical depth. 1, 4–6, 11–14,
XGBoost
          extreme gradient boosting. 1, 13, 14
```



Introduction

Major ecosystems of the world—boreal forests, shrublands, grasslands, and savannas—experience recurrent fires driven by natural causes or human activities (Di Giuseppe et al., 2016, 2021; Hantson et al., 2022). While fire weather components, such as temperature, have shown an increasing trend from the early 1980s to the present (Burton et al., 2024; El Garroussi et al., 2024), burnt areas trends have declined over the same period (Burton et al., 2024). This offset between worsening fire weather and reduced burnt areas reflects the influence of human activities, such as agricultural expansion, land-use changes, and fire suppression, in modulating fire outcomes (Abatzoglou et al., 2025). These contrasting trends have generated significant interest in understanding fire behaviour in relation to fuel characteristics, availability, and distribution (Carmona-Moreno et al., 2005; Hood et al., 2022). Fuel moisture remains one of the most influential determinants of fire danger; however, its observation is limited by the sparse, labour-intensive nature of in-situ sampling. Field measurements typically rely on destructive sampling of vegetation, which is costly to sustain over large areas and introduces methodological inconsistencies and observational uncertainty (Yebra et al., 2024). For instance, recent empirical work in the United Kingdom has shown that point-scale fuel moisture measurements often fail to capture the heterogeneity of surrounding landscapes, leading to substantial spatial mismatches even in ecosystems that appear relatively homogeneous (Little et al., 2024; Ivison et al., 2024, 2025). These limitations underscore the need for spatially continuous, observation-driven estimates of fuel moisture that can be integrated with fire danger rating systems and atmospheric monitoring frameworks that incorporate biomass-burning emissions (Fleming et al., 2009).

Recently, ECMWF developed a diagnostic fuel framework that integrates land-surface modelling, meteorological variables, and satellite observations (McNorton and Di Giuseppe, 2024). This system provides daily global updates of vegetation characteristics at 9 km resolution, including attributes of live and dead foliage and woody components. These fuel descriptors support the SPARKY probability of fire (PoF) model (McNorton et al., 2024; Di Giuseppe et al., 2025), which currently relies on a climatological LAI field to represent vegetation structure. While this offers a stable baseline, its predictive skill can be limited during anomalous seasons or rapid vegetation changes. Incorporating Earth observation (EO) data through data assimilation has the potential to replace the climatological constraint with dynamically evolving vegetation states, thereby improving both the timeliness and relevance of SPARKY-PoF for near-real-time fire forecasting and monitoring.

Efforts to address this limitation have highlighted the value of assimilating satellite-derived variables to better capture vegetation dynamics in land-surface models (Rosnay et al., 2013; Al-Yaari et al., 2014; Kumar et al., 2019; Garrigues et al., 2025). Building on this principle, the Fuelity project combines complementary observations, VOD-L and SIF, to improve estimates of key fuel properties. A central component of data assimilation (DA) is the observation operator, which translates model variables into observational space (Courtier et al., 1994). The choice of observation operator strongly influences assimilation performance and spans several approaches, including physical forward models, empirical operators, and data-driven emulators. Physical forward models rely on established physical principles to simulate the measurement process; for example, radiative transfer models that describe the interaction of radiation with vegetation canopies and soils (Verhoef, 1984; Jacquemoud and Baret, 1990; Widlowski et al., 2015). These models offer high fidelity and physical consistency but are computationally demanding, making their application challenging at global scales or high spatial resolution. Empirical observation operators, on the other hand, exploit statistical relationships derived from historical data, such as cumulative distribution function (CDF) matching, to map model states to observations. Such methods are computationally efficient and straightforward to implement (Calvet et al., 2023; Reichle and Koster, 2004; Drusch and Viterbo, 2007), but they may oversimplify nonlinear or heterogeneous



processes. More recently, data-driven emulators, including machine learning (ML) approaches, have emerged as powerful alternatives. These methods do not require explicit physical descriptions and can capture complex, nonlinear relationships in the observational data space, which is particularly advantageous for vegetation-related variables (Reichstein et al., 2019; Camps-Valls et al., 2021; Bonan et al., 2023). ML-based operators therefore provide a flexible and computationally efficient route to representing processes that are otherwise difficult to model explicitly.

In this report, we outline the Fuelity framework designed to improve LFMC by updating LAI and soil moisture in the SPARKY formulation using the SEKF within the ECMWF ecLand–IFS system. Section I introduces the datasets and satellite products used in this work. Section II describes the data assimilation framework, including the observation operators and SEKF configuration. Section III presents the results, assessing the impact of the updated fuel states on vegetation dynamics, fire forecasting, and numerical weather prediction.

1 Data

1.1 Satellite datasets

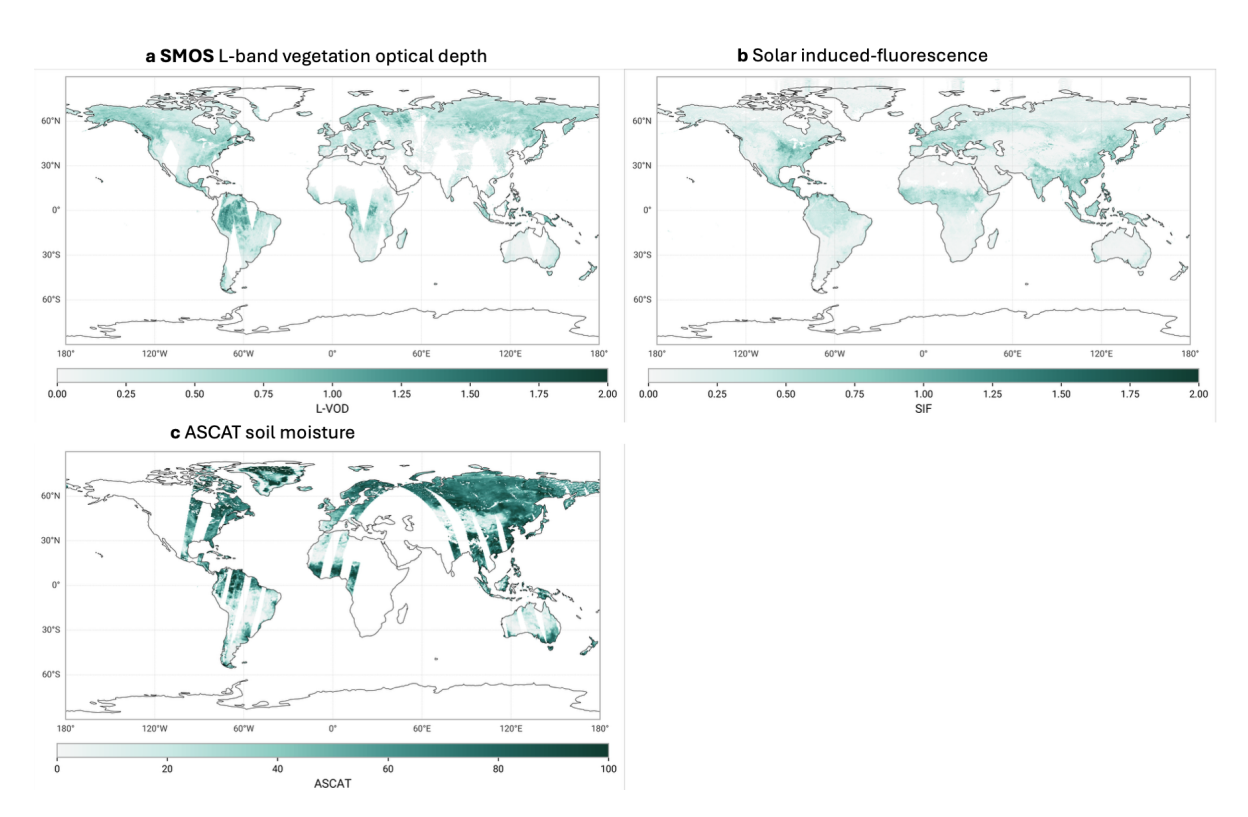


Figure 1: Satellite-derived datasets used in this study. Panels show global snapshots for August 2021 from: **a** SMOS L-band Vegetation Optical Depth (L-VOD), **b** TROPOMI Solar-Induced Fluorescence (SIF), and **c** ASCAT surface soil moisture.

In this study, we use three satellite-derived variables that capture complementary aspects of the vegetation—water system relevant to fuel dynamics: VOD-L (Fig. 1a), SIF (Fig. 1b), and near-surface soil moisture from ASCAT (Fig. 1c).

The variables, listed in Table 1, are retrieved from distinct satellite missions: VOD-L from SMOS MI-



RAS radiances, SIF from the TROPOMI spectrometer, and soil moisture from ASCAT C-band radar observations. L-band VOD-L (1.41 GHz) represents the attenuation of the microwave signal as it propagates through the canopy. The degree of attenuation increases with canopy water content and biomass, making VOD-L a physically based measure of vegetation optical thickness at microwave wavelengths. The long wavelength of L-band reduces saturation effects and enables deeper canopy penetration, giving VOD-L strong sensitivity to above-ground biomass and vegetation water content (Rodríguez-Fernández et al., 2018; Ulaby et al., 1981). As such, it provides a robust proxy for changes in live fuel moisture and canopy structure. ASCAT soil moisture is retrieved from C-band radar backscatter and reflects variations in near-surface soil water availability. Although vegetation contributes to the signal, ASCAT-based retrieval algorithms primarily respond to soil dielectric properties, providing reliable estimates of surface soil moisture. Because soil moisture constrains plant water uptake, ASCAT soil moisture offers essential information on the hydrological conditions influencing live fuel moisture. SIF provides an independent constraint on vegetation physiological activity by measuring the weak chlorophyll fluorescence emitted during photosynthesis. SIF depends on absorbed photosynthetically active radiation and photosynthetic efficiency, and it declines under water stress and stomatal closure (Guanter et al., 2021). It therefore offers a sensitive indicator of early vegetation stress and fuel desiccation.

Variable SIF VOD-L **ASCAT Soil Moisture** Satellite **SMOS** Sentinel-5P MetOp-A/B/C Sensor **MIRAS TROPOMI ASCAT** Frequency band (GHz) L-band (1.41) NIR (743-758 nm window) C-band (5.255) Swath (km) 1000 2600 550 **Spatial resolution (km)** 25 3.5×5.5 12.5 - 25**Temporal resolution** daily 8-daily daily Reference Al Bitar et al. (2017) Guanter et al. (2021) Wagner et al. (2013)

Table 1: Characteristics of the global satellite-derived variables used in this study.

1.2 Model datasets

1.2.1 ECMWF land surface model - ecLand

The ECMWF land-surface modelling system, ecLand, is based on the HTESSEL (Hydrology Tiled ECMWF Scheme for Surface Exchanges over Land) model (Balsamo et al., 2009; Boussetta et al., 2021), which represents vertical movements of soil moisture using the equations of Richards (1931). The soil column is discretised into four layers with thicknesses of 0.07, 0.21, 0.72, and 1.89 m from top to bottom. The vegetation representation in ecLand relies on a tile approach that accounts for dominant low (grassland, crop, shrubland) and high (forest) vegetation. In the current version of ecLand used in the IFS, vegetation parameters such as LAI are specified as seasonally varying climatological monthly mean maps in the ECMWF numerical weather prediction (NWP) system. This climatology uses the latest Copernicus Land Monitoring Service (CLMS) LAI dataset (1993-2019) from the CONFESS project (Boussetta and Balsamo, 2021) and has been shown to have a significant impact on quality. One of the main weaknesses of the current approach is that inter-annual variability in vegetation is not taken into account. Year-to-year differences in vegetation can be significant, driven most notably by land use change, as well as by fire events, meteorological extremes such as droughts or above-average rainfall, and fluctuations in 2-metre air temperature. These variations have become even more pronounced in recent years due to the effects of climate change. Soil moisture estimates could benefit from incorporating dynamic vegetation indicators like LAI, which can help update soil moisture by providing more accurate,



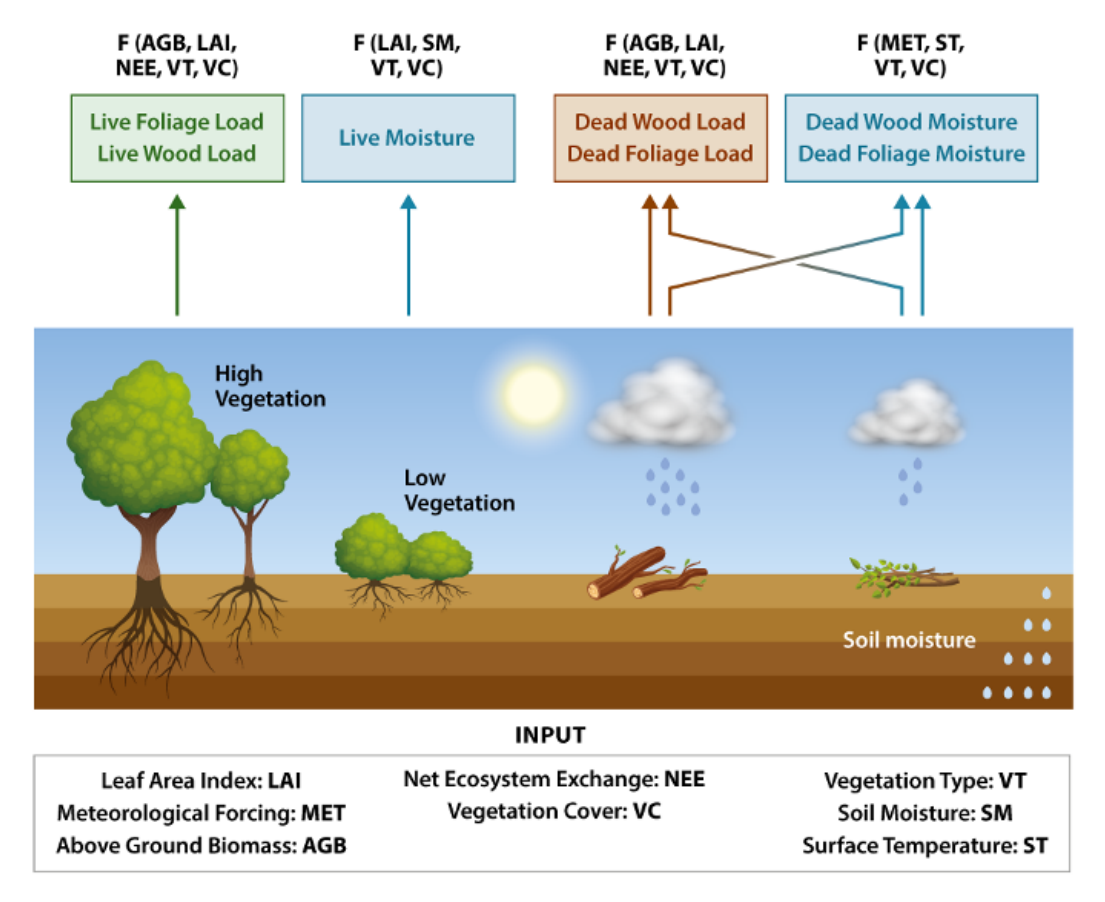


Figure 2: A schematic of the SPARKY-fuel model, illustrating the required input data and the dependencies for the output variables.

seasonally relevant vegetation states. These differences tend to be especially large during the transition seasons, spring and autumn, when vegetation characteristics change most rapidly as part of the annual cycle. This is particularly true in mid-latitude regions, where seasonal conditions vary the most.

1.2.2 SPARKY

SPARKY (McNorton and Di Giuseppe, 2024) is a diagnostic fuel model developed at ECMWF to provide spatially and temporally resolved estimates of live and dead fuel properties for wildfire danger prediction (see Fig. 2). It combines ecLand land-surface prognostic variables (including soil moisture, LAI, vegetation biomass, and meteorological drivers) with empirical and process-based formulations to estimate LFMC, dead fuel moisture, fuel load, and derived quantities relevant to fire behaviour. SPARKY partitions vegetation into structural components (e.g., foliage, fine woody material, coarse woody material) and computes moisture states for live and dead categories using physically informed relationships that link vegetation water status, atmospheric demand, and soil moisture availability. The live component relies primarily on ecLand leaf area index, canopy water content proxies, and environmental stress indices, whereas the dead component is driven by vapour pressure deficit, temperature, relative humidity, and surface moisture dynamics. These fuel properties are then passed to the SPARKY-PoF (McNorton et al., 2024) diagnostic to characterise fire danger. Because SPARKY is diagnostic, its accuracy depends strongly on the realism of the underlying vegetation and soil moisture states.



1.3 Independent validation datasets

1.3.1 Satellite-derived LAI observations

For vegetation, we use the observed CLMS LAI 300 m product (Verger et al., 2019), which provides 10-day global composites at 300 m resolution and is widely used for ecosystem monitoring and land-surface modelling. The consolidated RT6 version was resampled to an 8-day frequency to align with the temporal resolution of the SIF observations assimilated in this work.

Although CLMS LAI 300 m offers high spatial detail and operational continuity, the reliance on machinelearning inversion introduces several limitations, including sensitivity to the training domain, residual inconsistencies under dense canopies, and potential artefacts during rapid vegetation transitions. Additional structural changes were introduced in July 2020, when Sentinel-3 OLCI replaced PROBA-V as the primary sensor, modifying the spectral inputs and influencing the temporal consistency of the retrievals. This is particularly relevant here because the CONFESS project's LAI climatology (Boussetta and Balsamo, 2021) was based on the GEOV2 long-term LAI dataset (Baret et al., 2013), which merges SPOT-VGT (1999-2014) and PROBA-V (2014-2019). Consequently, the 2021 CLMS LAI fields differ from the CONFESS climatology due to interannual variability, the transition from PROBA-V to Sentinel-3, and changes in the retrieval methodology. To ensure consistency with the long-term CON-FESS record, the CLMS LAI was bias-corrected before use. This correction was performed using a machine-learning approach comparable to the CDF-matching method applied in CONFESS (Boussetta and Balsamo, 2021). To characterise vegetation seasonality, we derived the 2021 amplitude of the biascorrected CLMS LAI 300 m product, calculated as the difference between the annual maximum and minimum LAI after resampling to an 8-day frequency (Fig. 3). The resulting map shows large seasonal variations across temperate, boreal, and semi-arid regions, and comparatively low variability in tropical evergreen forests. This provides a reference for the magnitude and spatial pattern of observed LAI dynamics used in the assimilation framework.

1.3.2 ISMN in situ soil moisture observations

For soil moisture, we used in situ observations from the international soil moisture network (ISMN) (Dorigo et al., 2021), which compiles quality-controlled point measurements from multiple regional and national monitoring networks. These ground-based observations serve as a reference standard for assessing the accuracy of satellite- and model-derived surface soil moisture estimates.

1.3.3 MODIS active fires

Active fire detections were obtained from the MODIS Collection 6.1 Active Fire product, which provides globally consistent observations of thermal anomalies derived from the 1 km fire channels on board the Terra and Aqua satellites. The algorithm identifies actively burning pixels using contextual tests that compare the thermal signal of each pixel with that of its surrounding neighbourhood, enabling robust discrimination between fires and other hot surfaces. MODIS active-fire detections are widely used for global fire monitoring due to their long observational record, twice-daily sampling from the combined platforms, and rigorous calibration and validation. Although the product inevitably misses small or short-lived fires and may be affected by cloud cover and overpasses, it remains one of the most reliable long-term datasets for characterising fire occurrence and timing at regional to global scales.

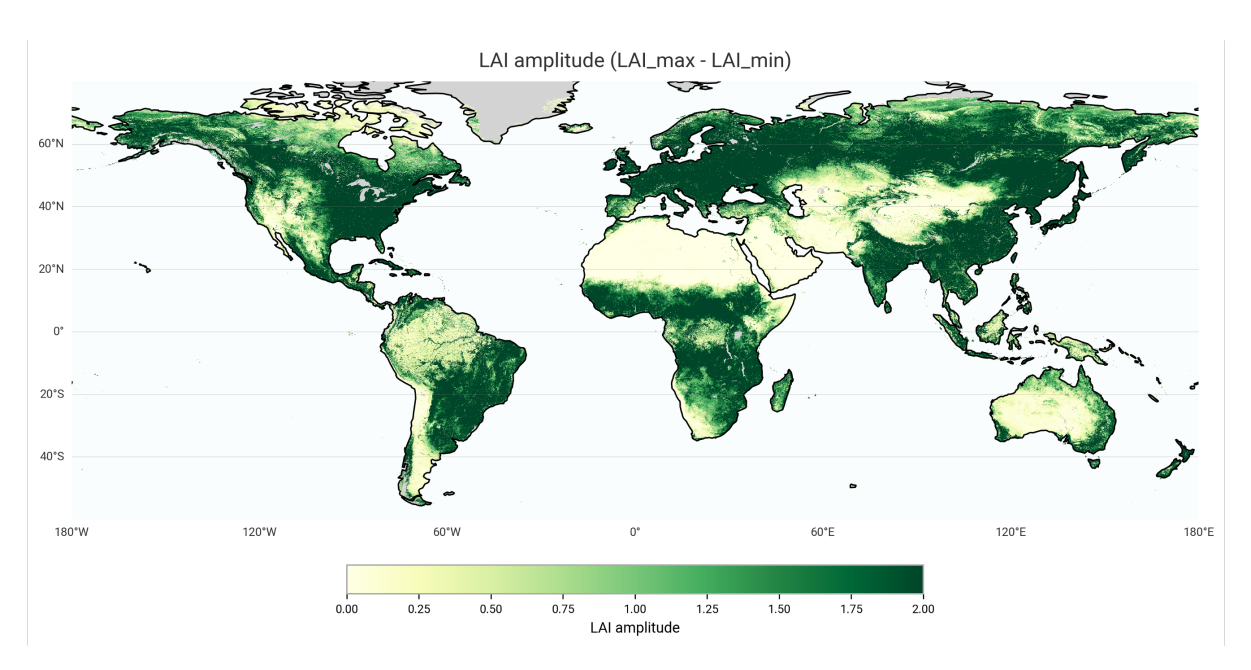


Figure 3: Global seasonal amplitude of the CLMS 300 m LAI product, computed as the difference between the annual maximum and minimum LAI after resampling to an 8-day temporal frequency. High amplitudes in temperate and boreal forests, savannas, and semi-arid regions reflect strong seasonal cycles in canopy development and senescence, whereas tropical evergreen forests exhibit markedly lower variability.

2 Methodology

2.1 Live fuel moisture derivation

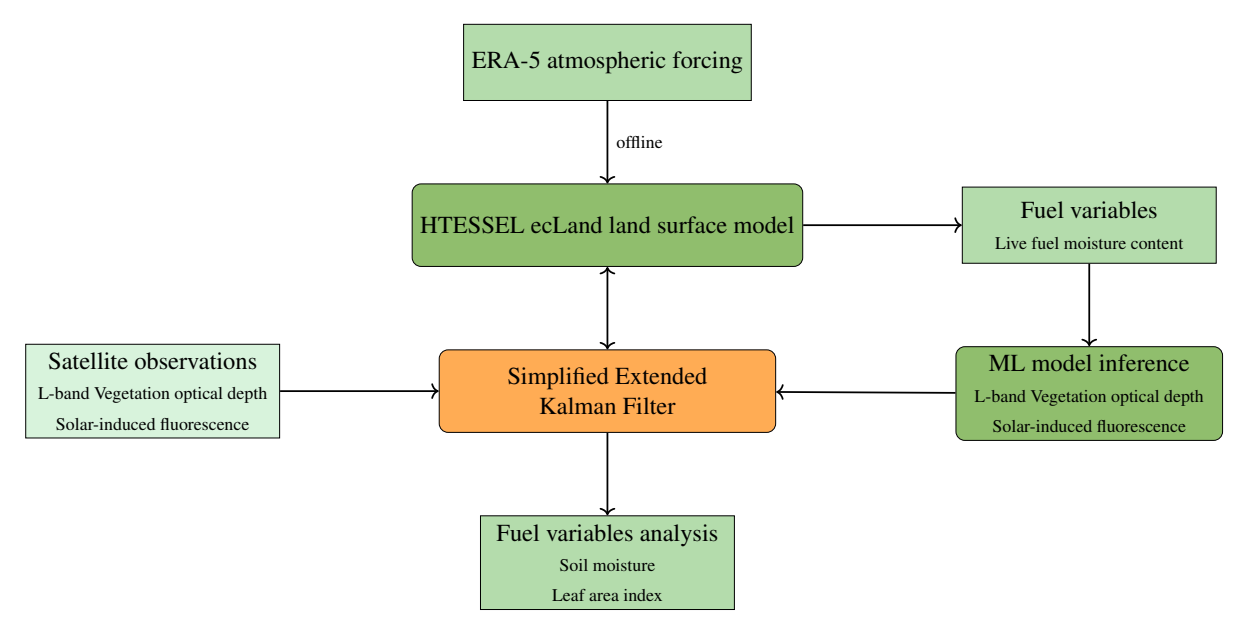
The SPARKY (see section 1.2.2) formulation was used to derive LFMC from LAIs and soil moisture, treating these variables as proxies for canopy water status and vegetation condition. A semi-empirical model was fitted using Globe-LFMC samples to estimate LFMC globally at a daily 9 km resolution. The model assumes an asymptotic response of LFMC to LAI and soil moisture and is expressed as:

$$LFMC = LFMC_{max} - Ae^{-(\alpha LAI + \beta SM + \gamma LAI \cdot SM)}, \tag{1}$$

where LFMC_{max} represents the vegetation-specific upper bound of LFMC and A denotes the range between minimum and maximum values. The coefficients α , β , and γ govern the sensitivities to soil moisture, LAI, and their interaction, respectively, capturing drought resistance and growing-season uptake effects within a compact formulation. Parameters were estimated using a trust-region reflective optimisation applied separately to seven vegetation functional types (crops, short grass, evergreen needleleaf forest, deciduous broadleaf forest, mixed crops–grassland, deciduous shrubs, and broadleaf savanna) based on subsamples of the Globe-LFMC dataset. The remaining types were assigned the closest analogue. LAI was obtained from the CONFESS dataset (Boussetta and Balsamo, 2021) at a monthly 9 km resolution, and soil moisture was sourced from ERA5-Land (Muñoz-Sabater et al., 2021), aggregated according to ecLand rooting-depth distributions (Boussetta et al., 2021).



2.2 Land data assimilation framework



LFMC: diagnostic based on LAI and SM

Figure 4: Schematic of the data assimilation system for LAI analysis: Satellite observations of VOD-L and SIF are assimilated using SEKF to update LAI, from which LFMC is diagnosed. A machine learning-based observation operator is used to map model variables to observation space.

In the system implemented for this study, we use an offline DA setup (except for Section 3.3.3, where online DA is used to evaluate the impact on NWP skill), meaning that the analysis corrections do not feed back into the atmospheric forcing (de Rosnay et al., 2022). The state vector includes soil moisture from the top three soil layers ($SM_{l1:3}$) and LAI. For the computation of the LFMC analysis, increments of LAI and the three top layers were applied; no increment was applied to the deepest soil layer (SM_{l4}).

The observation vector, background state vector, and observation operator are structured as follows:

$$\mathbf{y}^{\mathbf{o}} = \begin{bmatrix} 2mT \\ 2mRH \\ ASCAT \\ VOD_L \\ SIF \end{bmatrix} \qquad \mathbf{x}^{b} = \begin{bmatrix} SM_{l1} \\ SM_{l2} \\ SM_{l3} \\ LAI \end{bmatrix} \qquad \mathcal{H}(\mathbf{x}^{b}) = \begin{bmatrix} 2mT \\ 2mRH \\ SM_{top} \\ VOD_{L,b} \\ SIF_{b} \end{bmatrix}$$
(2)

We use the notation VOD_L instead of "VOD-L" in mathematical formulations to avoid confusion with a minus sign.

In Equation 2, variables highlighted in orange represent the existing observations and model states already assimilated into the system. Specifically, 2-metre temperature (2mT) and 2-metre relative humidity (2mRH) pseudo-observations, along with ASCAT soil moisture observations, were assimilated to improve soil moisture estimates in the top three model layers. Variables highlighted in purple correspond to the newly assimilated datasets introduced in this study, specifically VOD-L and SIF, to enhance the representation of LAI.



As described in Drusch et al. (2009), the background error covariance matrix (**B**) and the observation error covariance matrix (**R**) were assumed to be static and diagonal, with diagonal terms defined by error variances (σ_b^2 for background errors and σ_o^2 for observation errors). The values in Table 2 represent the final configuration retained for the assimilation system. They were selected based on sensitivity experiments in which background and observation standard deviations were systematically varied to assess their impact on assimilation performance. A larger observation error (σ_o) results in smaller analysis increments, giving more weight to the background, while smaller observation errors increase the influence of observations. Similarly, larger background errors (σ_b) increase the weight of observations in the analysis.

Table 2: Standard deviation values (σ_b for background errors and σ_o for observation errors) retained for this study. These values define the diagonal terms of the background error covariance matrix (\mathbf{B}) and the observation error covariance matrix (\mathbf{R}).

Variable	Standard Deviation	Unit
Background variables (σ_b)		
Soil moisture (top three layers)	0.01	$\mathrm{m^3~m^{-3}}$
LAI	1	$\mathrm{m}^2~\mathrm{m}^{-2}$
Observation variables (σ_o)		
2-metre temperature	1	K
2-metre relative humidity	4	%
ASCAT soil moisture	0.05	$\mathrm{m}^3~\mathrm{m}^{-3}$
VOD-L	0.16	unitless
SIF	0.12	${ m mW} { m m}^{-2} { m sr}^{-1} { m nm}^{-1}$

Background errors for soil moisture, 2-metre temperature, 2-metre relative humidity, and ASCAT soil moisture follow the statistics reported in K. Scipal, M. Drusch, and W. Wagner (2008); Rosnay et al. (2013). The LAI background error standard deviation was set to a static value of 1 m² m⁻² based on sensitivity analysis and is consistent with literature reporting typical static LAI errors in the 0.4–1.2 m² m⁻² range (Sabater et al., 2008; Albergel et al., 2018; Barbu et al., 2011; Garrigues et al., 2025). LAI was assimilated against a climatological background representing the mean seasonal cycle, which does not capture interannual or synoptic variability. Its associated uncertainty was intentionally inflated toward the upper range of literature values to reflect spatial heterogeneity, model structural limitations, and observation–model mismatches. Assigning a larger background error allows the analysis to place greater weight on observational information. Observation error standard deviations for SIF and VOD-L were derived from O–B statistics over the year 2021. Desroziers diagnostics Desroziers et al. (2005) applied to single-observation-type assimilation experiments indicated similar error magnitudes despite imperfect convergence.

The Jacobian matrix **H** was computed via finite differences as follows:

$$\mathbf{H} = \begin{bmatrix} \frac{T_{2m_pert1} - T_{2m}}{\delta SM_{l1}} & \frac{T_{2m_pert2} - T_{2m}}{\delta SM_{l2}} & \frac{T_{2m_pert3} - T_{2m}}{\delta SM_{l3}} & \frac{T_{2m_pert4} - T_{2m}}{\delta SM_{l3}} \\ \frac{RH_{2m_pert1} - RH_{2m}}{\delta SM_{l1}} & \frac{RH_{2m_pert2} - RH_{2m}}{\delta SM_{l2}} & \frac{RH_{2m_pert3} - RH_{2m}}{\delta SM_{l3}} & \frac{RH_{2m_pert4} - RH_{2m}}{\delta SM_{l3}} \\ \frac{SM_{l1_pert1} - SM_{l1_ASCAT}}{\delta SM_{l1}} & \frac{SM_{l1_pert2} - SM_{l1_ASCAT}}{\delta SM_{l2}} & \frac{SM_{l1_pert3} - SM_{l1_ASCAT}}{\delta SM_{l3}} & \frac{SM_{l1_pert4} - RH_{2m}}{\delta LAI} \\ \frac{VOD_{L_pert1} - VOD_{L}}{\delta SM_{l1}} & \frac{VOD_{L_pert2} - VOD_{L}}{\delta SM_{l2}} & \frac{VOD_{L_pert3} - VOD_{L}}{\delta SM_{l3}} & \frac{VOD_{L_pert4} - VOD_{L}}{\delta LAI} \\ \frac{SIF_{pert4} - SIF}{\delta SM_{l1}} & \frac{SIF_{pert2} - SIF}{\delta SM_{l2}} & \frac{SIF_{pert3} - SIF}{\delta SM_{l3}} & \frac{SIF_{pert4} - SIF}{\delta LAI} \end{bmatrix}$$



Following Drusch et al. (2009), the soil moisture perturbations ($\delta SM_{l1:3}$) were set to 0.01 m³m⁻³. Similarly, the LAI perturbation (δLAI) was set to 0.01 m² m⁻² based on sensitivity analysis.

In this study, the assimilation of VOD-L and SIF was intentionally restricted to updating only the LAI component of the state vector, with their sensitivities (Jacobians) with respect to soil moisture set to zero.

Table 3: Summary of XGBoost features.

Variable	Input Category	Frequency	Source	Reference
2m Temperature (2t)	Weather	Daily	ERA5-Land	Muñoz Sabater et al. (2021)
2m Dewpoint Temperature (2d)	Weather	Daily	ERA5-Land	Muñoz Sabater et al. (2021)
Surface Short-wave (solar) Radiation Downwards (ssrd)	Weather	Daily (acc.)	ERA5-Land	Muñoz Sabater et al. (2021)
Soil Moisture (swvl)	Weather/Fuel	Daily	ERA5-Land	Muñoz Sabater et al. (2021)
Soil Temperature (stl)	Weather	Daily	ERA5-Land	Muñoz Sabater et al. (2021)
Total Fuel Load	Fuel	Daily	Fuel Model	McNorton and Di Giuseppe (2024)
Dead Fuel Moisture Content	Fuel	Daily	Fuel Model	McNorton and Di Giuseppe (2024)
Leaf Area Index (LAI)	Fuel/Vegetation	10-daily	Satellite (Copernicus Global Land Service, LAI 300m v1.0)	Fuster et al. (2020)
Type of Vegetation	Vegetation	Fixed	ecLand	Boussetta et al. (2021)
Vegetation Cover	Vegetation	Fixed	ecLand	Boussetta et al. (2021)



2.3 Observation operators

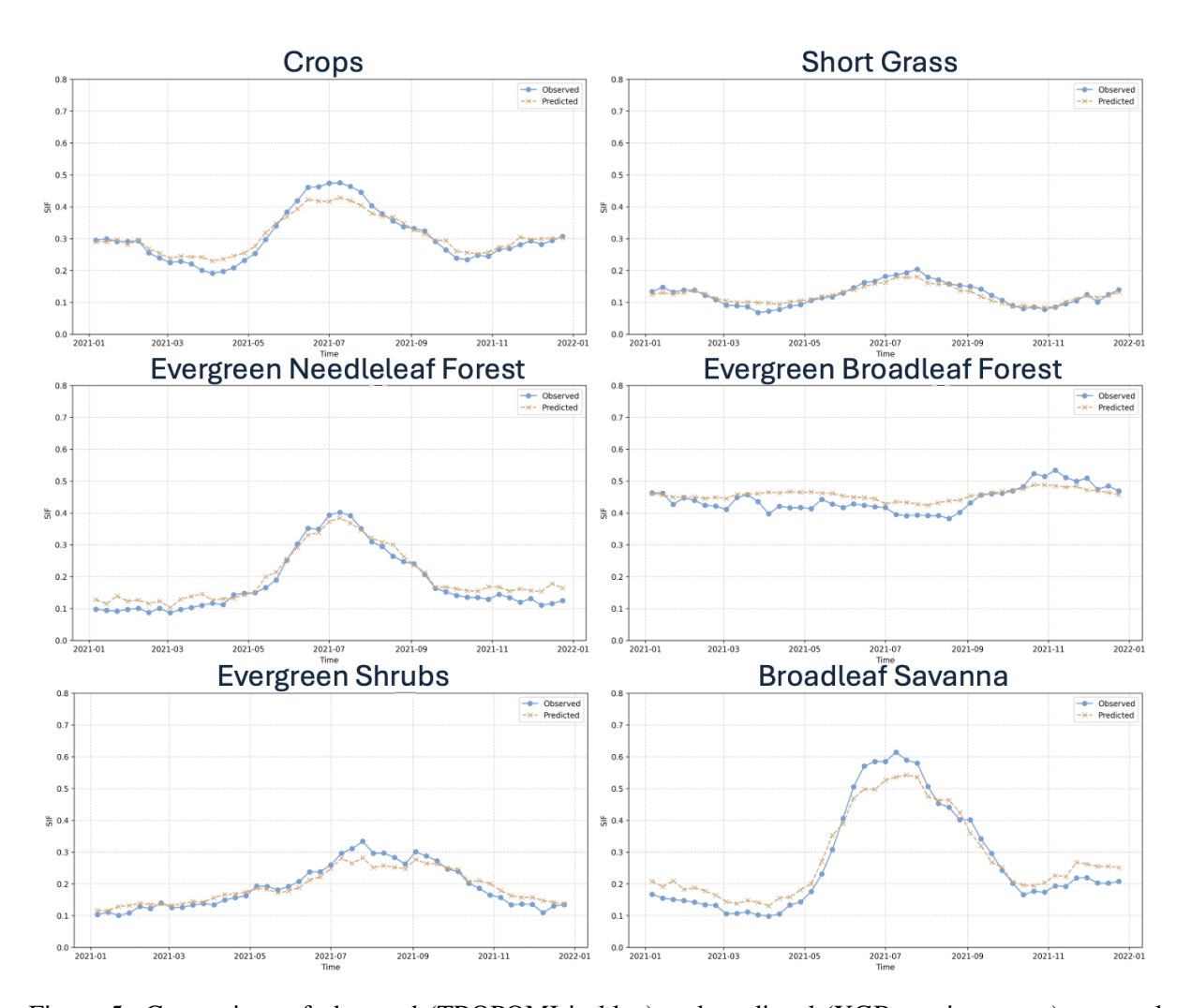


Figure 5: Comparison of observed (TROPOMI in blue) and predicted (XGBoost in orange) seasonal cycles of SIF across major vegetation types in 2021. The XGBoost model closely reproduces the satellite-derived seasonal cycle for six representative biomes, accurately capturing both the phasing and amplitude of seasonal variations.

Two machine learning models were developed as ML-based observation operators, XGBoost and MLP, and trained to predict the model-space equivalents of satellite SIF and L-band VOD-L using a common predictor set. Their predictive performance was broadly comparable; however XGBoost was selected for integration into the assimilation framework due to its numerical stability, ease of implementation, and greater interpretability, which supported the verification of physically consistent predictor–response relationships. The XGBoost operator was trained on 8-day data for 2019–2020, matching the temporal frequency of SIF, and evaluated using an independent dataset from 2021. Predictors were temporally aligned with the satellite record and preprocessed to ensure internal consistency. The final set (Table 3) comprises fuel-related variables, LAI, surface and deep soil moisture, near-surface meteorological conditions, and vegetation-type information. LAI from the CLMS 300 m product was resampled to an 8-day cycle, and all experiments were conducted at TCO1279 (\simeq 9 km) resolution. Regularisation parameters were tuned to maintain stable behaviour across biomes, using a split penalty of $\gamma = 2.0$, L_2 and L_1



terms of $\lambda = 5.0$ and $\alpha = 2.0$, a minimum child weight of 10, and a subsampling fraction of 0.6. An avenue for further development is to compare the analytically derived Jacobians available from the MLP with finite-difference Jacobians computed from the XGBoost operator to assess their consistency and potential suitability for future assimilation configurations.

3 Results

3.1 Observation operator performance

The XGBoost-based observation operator reproduced the satellite-driven seasonal cycle for both SIF and VOD-L across major vegetation types. Validation against an independent 2021 dataset showed that LAI explained 67% of the variance in SIF and 72% in VOD-L, with RMSE values of 0.12 and 0.16 m²m⁻², indicating strong sensitivity to vegetation structure and seasonal dynamics. Figure 5 illustrates this behaviour for SIF, showing close agreement between observed and predicted seasonal cycles across six representative biomes. The operator captured the timing and amplitude of the annual cycle, including pronounced mid-year peaks in crops and savannas, as well as weaker variability in evergreen systems.

3.2 25-year live fuel moisture reanalysis

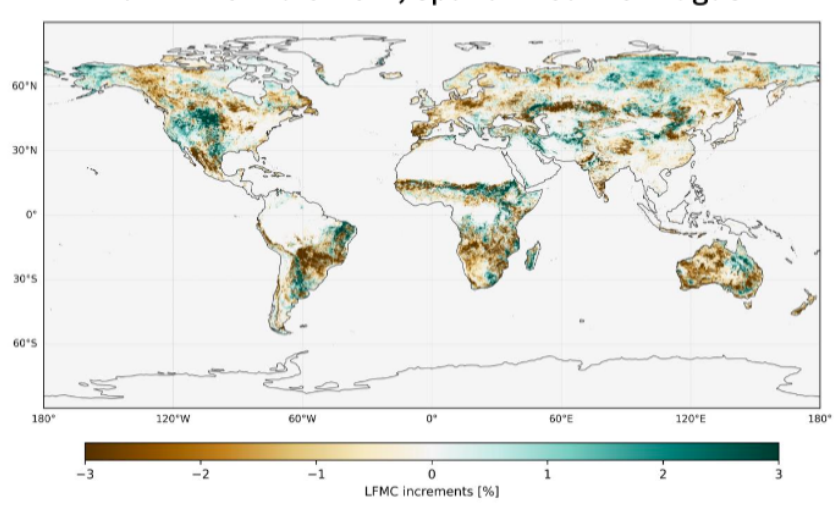
The assimilation system was first evaluated for 2021 to assess its impact on vegetation and soil states. Comparisons with ISMN showed that the increments applied to surface soil moisture were small and did not yield systematic improvements. In contrast, assimilating SIF and VOD-L produced substantial adjustments to the LAI climatology, correcting its amplitude and phase to reflect the observed seasonal cycle and interannual variability. This improvement provided a basis for applying the system over a longer period to produce a multi-decadal record of LFMC. The assimilation was therefore applied from 1999 to 2024 to produce a 25-year satellite-informed LFMC reconstruction at approximately 9 km resolution. When LAI-related satellite observations were unavailable—particularly before the launch of SMOS and TROPOMI—the system relied on the CLMS LAI product to maintain continuity in vegetation constraints. The resulting LAI analysis, together with the soil moisture field taken from ERA5-Land(Muñoz Sabater et al., 2021), was subsequently combined through Equation 1 to produce the updated LFMC. Figure 6a shows the spatial pattern of the mean LFMC increment for August, with positive corrections in boreal and temperate ecosystems where the climatological LAI underestimates peak-season greenness, and negative corrections in semi-arid regions where vegetation activity is overestimated. Figure 6b presents the corresponding LFMC anomalies over 2003 to 2022, highlighting coherent year-to-year variations driven by global drought patterns and shifts in vegetation productivity. Together, these results demonstrate that the assimilation provides physically consistent adjustments to vegetation state, enabling a long-term LFMC dataset that reflects both satellite-observed variability and model dynamics.

Table 4: Data availability for the LFMC reanalysis. The table lists the dataset produced in this study and the corresponding access link.

Dataset	Access
LFMC reanalysis (1999–2024)	10.24381/378d1497
XGBoost model	Github/Fuelity/XGBoost



a LFMC increment, spatial mean for August



b LFMC anomaly – Reference period: 2003-2022

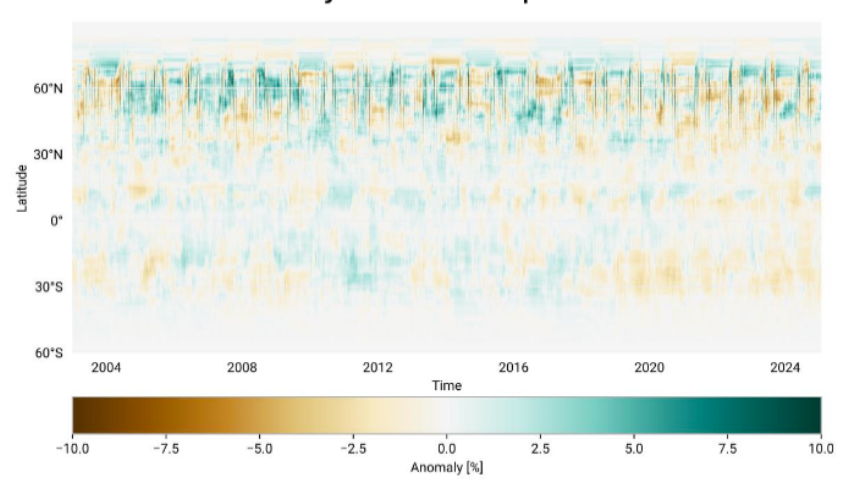


Figure 6: Assimilation-driven adjustments and long-term variability in LFMC. **a** Spatial pattern of the mean LFMC increment for August, expressed as the difference between the analysis and model background. Positive increments indicate higher LFMC after assimilation, while negative increments indicate reductions. **b** Latitude–time distribution of LFMC anomalies for 2003–2022, computed relative to the 20-year reference climatology. Colours represent departures from the long-term mean LFMC at each latitude.



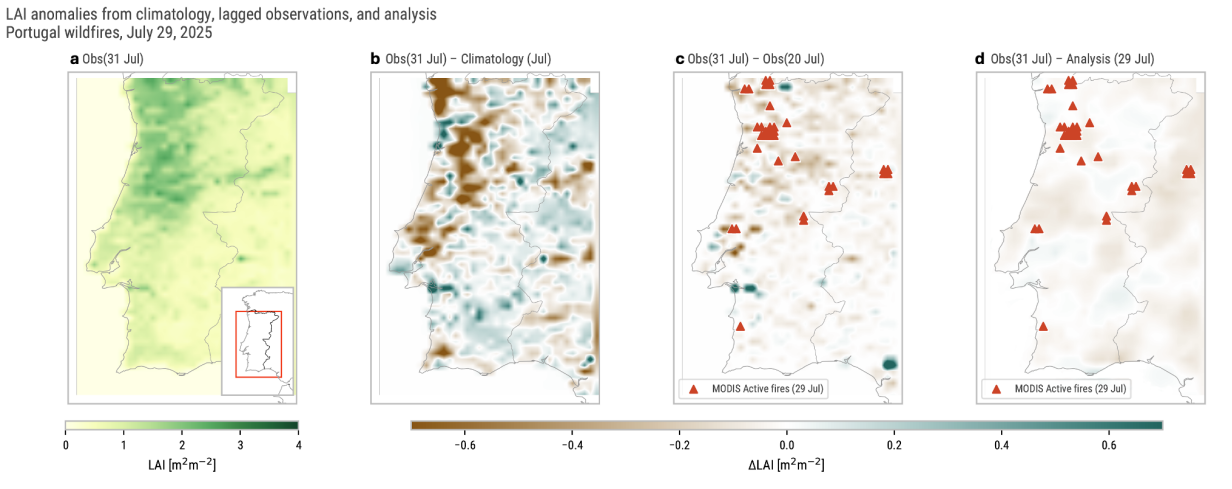


Figure 7: LAI anomalies during the Portugal wildfires on 29 July 2025. **a** Bias-corrected CLMS LAI on 31 July. **b** LAI anomaly relative to the July climatology. **c** Change in LAI between 20 and 31 July, with MODIS active fires on 29 July. **d** Difference between observations on 31 July and the analysis on 29 July.

3.3 Impact evaluation

We assessed the impact of the assimilation on vegetation and surface conditions during the 2025 boreal summer (June–August), a period characterised by strong seasonal gradients in fuel moisture and high fire activity across mid-latitude regions.

3.3.1 Vegetation dynamics

Late July 2025 in Portugal was marked by persistent heat and low humidity, with dry northerly winds limiting moisture availability across much of the country. Vegetation conditions reflected this pattern (Fig. 7). The first LAI observation available after the event, on 31 July, shows a marked reduction in foliage over the affected areas. When compared with the July climatology (Fig. 7b), these observations reveal substantial negative anomalies, indicating the extent to which vegetation conditions had diverged from the long-term seasonal state under the prevailing meteorological conditions. Because the CLMS product is available only every 10 days, the change between 20 and 31 July (Fig. 7c) captures part of this decline but cannot fully resolve the progression of the canopy downturn. The analysis on 29 July (Fig. 7d) reduces this observational lag by adjusting the vegetation field towards the low-LAI state emerging during the event, providing a more representative estimate than either the climatology or the most recent observation.

3.3.2 Fire forecasting

To evaluate whether the behaviour identified in Portugal also appears across larger spatial scales, we conducted a regional analysis over the Mediterranean, where vegetation seasonality and fire occurrence differ markedly between subregions. We used the SPARKY PoF model with three LAI LAI "flavours" as inputs: climatological (CLIM), analysed (DA), and near-real-time observed from CLMS (NRT), and compared the resulting modelled signals with MODIS active-fire detections. Across the Western Mediter-

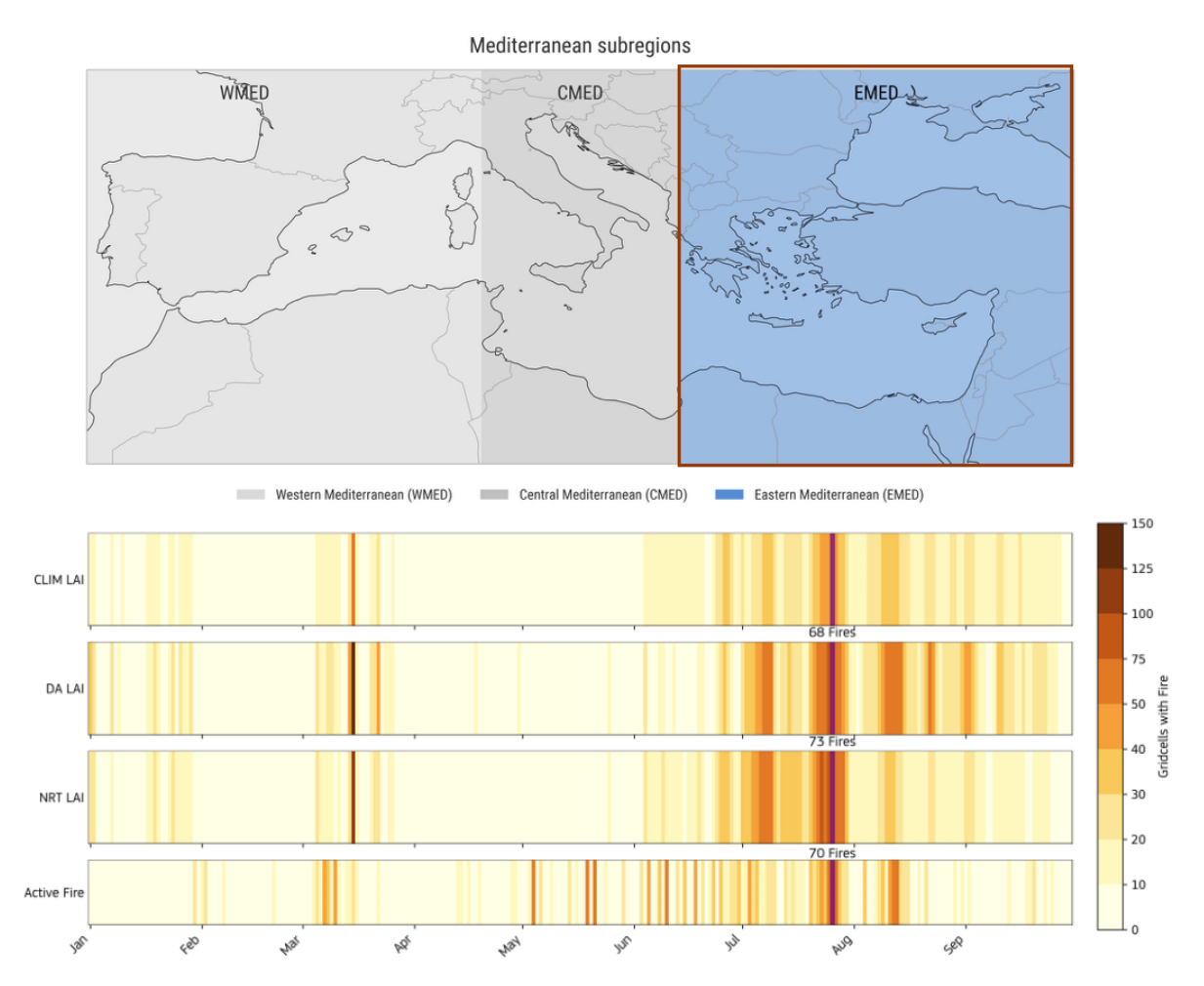


Figure 8: Sensitivity of SPARKY Probability-of-Fire (PoF) to different LAI forcings across the Mediterranean. Top: Definition of the Mediterranean subregions used in the analysis: Western (WMED), Central (CMED), and Eastern (EMED). Bottom: Regional time series of SPARKY-PoF forced by three LAI configurations: climatological LAI (CLIM), analysed LAI (DA), and near-real-time LAI (NRT), compared with MODIS active fire detections.



ranean (WMED) and Central Mediterranean (CMED), the three LAI configurations exhibit very similar seasonal behaviour, which is consistent with the weak vegetation seasonality characteristic of these regions. Consequently, the SPARKY-PoF curves produced using climatological, analysed, and NRT LAI differ only slightly, with each providing a comparable match to the observed pattern of fire activity. In contrast, the Eastern Mediterranean (EMED) (Fig. 8) shows a clearer separation between the LAI fields. The climatological LAI produces a smooth seasonal cycle and does not capture the sharper mid-summer reductions visible in the satellite record. The NRT and DA LAI forced PoF follow a more pronounced decline, with similar timing and magnitude.

When used as forcing for SPARKY-PoF, both the NRT and DA LAI configurations produce a stronger and more temporally aligned pre-fire increase in fire probability than the climatological LAI. The analysed LAI produces a slightly sharper transition due to the assimilation updates, but the overall behaviour is consistent between the two satellite-informed versions.

3.3.3 Numerical weather prediction

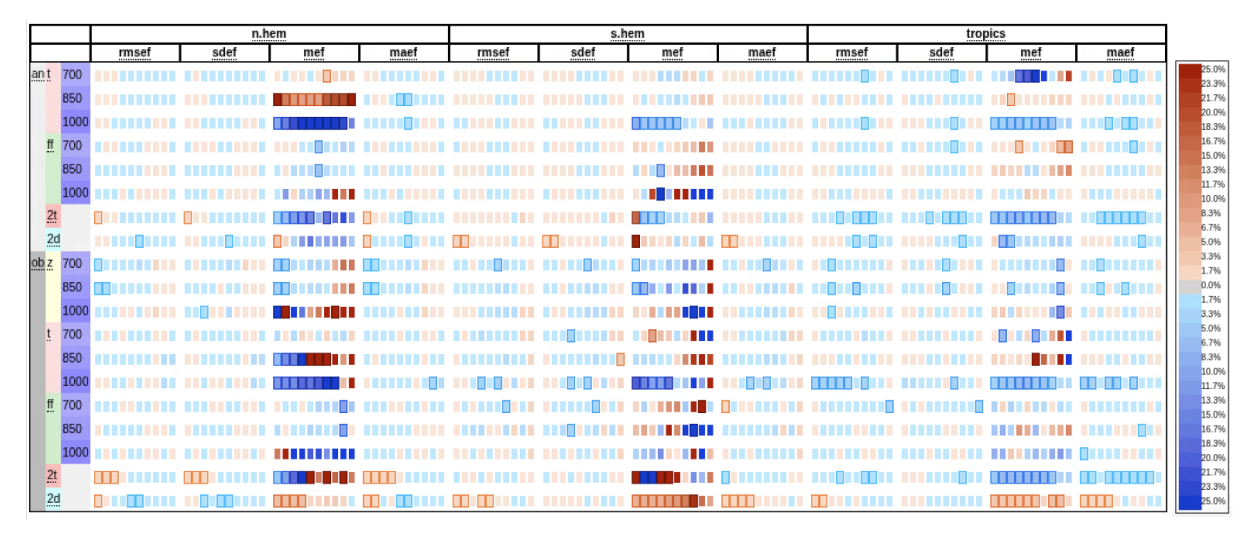


Figure 9: Verification scorecard for near-surface meteorological variables. Scorecard summarising the impact of using analysed LAI in the IFS compared to the climatological configuration for June–July–August 2025. Colours indicate changes in forecast skill across regions and 10-day lead times. Blue squares denote improved performance, while red squares indicate degradation. Only differences that pass a 95% significance threshold are shown.

Although NWP performance was not a primary objective of Fuelity, evaluating the atmospheric response to vegetation corrections is essential for understanding the broader implications of satellite-informed land states. We therefore performed online integrations of the IFS over June, July, and August, during which the analysed LAI replaced its climatological baseline. In this configuration, departures in vegetation state directly influence surface conductance, evapotranspiration, and the partitioning of available energy, allowing vegetation anomalies to feedback into near-surface meteorology. Across different global regions, the score fields display a systematic atmospheric response to the updated vegetation forcing (Fig. 9). In the Northern Hemisphere mid-latitudes, where the analysed LAI experiences widespread negative anomalies linked to early drying and canopy loss, the forecasts show warmer (Fig. 10) 1000 hPa and 2 m temperatures, along with lower 2 m dew-point temperatures (Fig. 11). This combination of higher temperatures and lower moisture is consistent with a boundary layer receiving less evaporative



cooling. Although surface fluxes were not explicitly diagnosed in this study, the pattern is physically indicative of reduced evapotranspiration and enhanced sensible heat flux. Such behaviour is expected when the canopy becomes sparser or water-limited, reducing transpiration and increasing the fraction of net radiation converted into turbulent heating of the near-surface air. The signal weakens in the Southern Hemisphere and the tropics, where differences between analysed and climatological LAI are smaller and vegetation phenology exerts less seasonal control on surface fluxes in the IFS.

Time-varying, observation-informed vegetation states can affect short-range forecasts. As parts of the IFS land scheme have been fine-tuned for the use of climatological LAI, adopting analysed vegetation states may require revisiting these routines and could explain the degradation in the 2 m dew-point.

While a systematic exploration of the full flux pathways lies beyond Fuelity's scope, the results high-light the broader relevance of vegetation analysis for coupled prediction systems and motivate further investigation into land–atmosphere feedbacks.

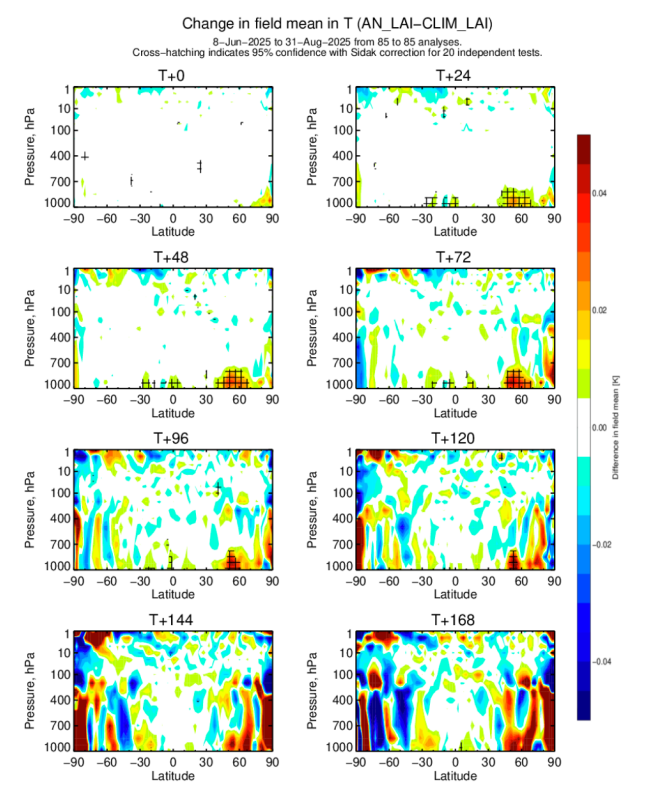


Figure 10: Latitude–pressure structure of temperature changes. The difference in mean temperature (DA-LAI - CLIM-LAI) for forecasts initialised between 1 June and 31 August 2025 is presented. Panels display latitude–pressure cross-sections at lead times ranging from 12 to 168 hours. Warm colours indicate higher temperatures in the experiment using analysed LAI, while cool colours denote lower values compared with the climatological-LAI configuration. Cross-hatching marks regions where the differences are significant at the 95% confidence level, using a Šidák correction for 20 independent tests.

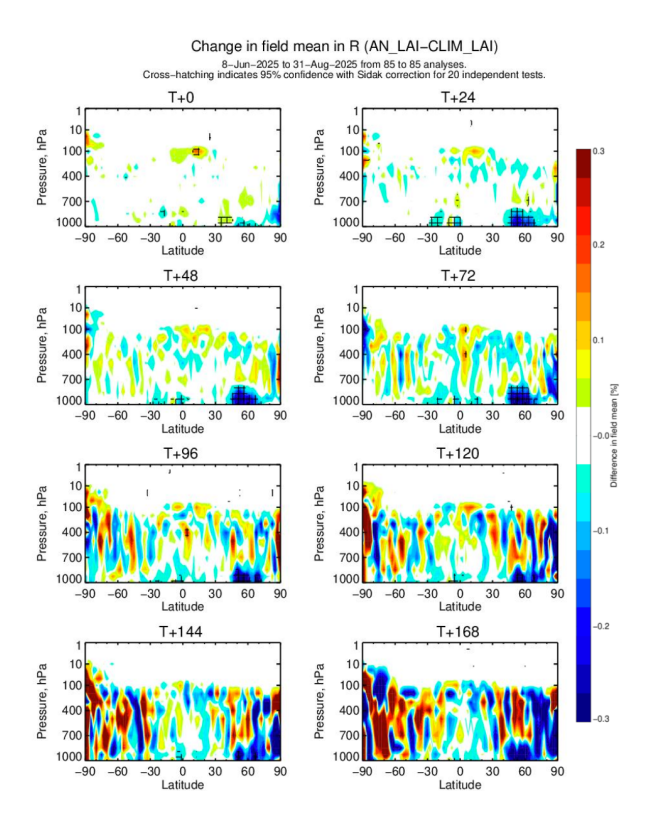


Figure 11: Latitude–pressure structure of the change in relative humidity. The difference in mean relative humidity (DA-LAI – CLIM-LAI) for forecasts initialised between 1 June and 31 August 2025 is presented. Panels display latitude–pressure cross-sections at lead times from 12 to 168 hours. Warm colours indicate higher relative humidity in the experiment using analysed LAI, while cool colours indicate lower values compared with the climatological-LAI configuration. Cross-hatching marks regions where the differences are significant at the 95% confidence level using a Šidák correction for 20 independent tests.

Conclusion

Fuelity has demonstrated that live fuel moisture is a critical driver of extreme fire behaviour; however, the scarcity of in-situ LFMC measurements forces operational systems to rely almost entirely on satellite observations. By showing that LAI—the primary large-scale proxy of LFMC—is observed only every 10 days and is therefore unable to capture rapid fuel transitions, Fuelity has leveraged additional observations such as VOD-L and SIF to improve our understanding of vegetation water content. Crucially, the project proved that linking these datasets requires a physical model, as purely observational methods introduce artefacts and inconsistencies, whereas a data-assimilation framework delivers physically coherent estimates across the full range of fuel variables. Fuelity's new LFMC product could provide accurate, real-time live fuel moisture information that substantially enhances existing fire danger datasets, and its success reinforces the Global Climate Observing System's recognition of LFMC as a priority variable to be added to the essential climate variables for monitoring climate-driven fire adaptation.



References

- Abatzoglou, J., Kolden, C., Cullen, A., Sadegh, M., Williams, E., Turco, M., and Jones, M.: Climate change has increased the odds of extreme regional forest fire years globally, Nature Communications, 16, https://doi.org/10.1038/s41467-025-61608-1, 2025.
- Al Bitar, A., Mialon, A., Kerr, Y. H., Cabot, F., Richaume, P., Jacquette, E., Quesney, A., Mahmoodi, A., Tarot, S., Parrens, M., Al-Yaari, A., Pellarin, T., Rodriguez-Fernandez, N., and Wigneron, J.-P.: The global SMOS Level 3 daily soil moisture and brightness temperature maps, Earth System Science Data, 9, 293–315, 2017.
- Al-Yaari, A., Wigneron, J.-P., Ducharne, A., Kerr, Y., de Rosnay, P., de Jeu, R., Govind, A., Al Bitar, A., Albergel, C., Muñoz-Sabater, J., Richaume, P., and Mialon, A.: Global-scale evaluation of two satellite-based passive microwave soil moisture datasets (SMOS and AMSR-E) with respect to Land Data Assimilation System estimates, Remote Sensing of Environment, 149, 181–195, https://doi.org/https://doi.org/10.1016/j.rse.2014.04.006, 2014.
- Albergel, C., Munier, S., Bocher, A., Bonan, B., Zheng, Y., Draper, C., Leroux, D. J., and Calvet, J.-C.: LDAS-Monde Sequential Assimilation of Satellite Derived Observations Applied to the Contiguous US: An ERA-5 Driven Reanalysis of the Land Surface Variables, Remote Sensing, 10, https://doi.org/10.3390/rs10101627, 2018.
- Balsamo, G., Viterbo, P., Beljaars, A., van den Hurk, B., Hirsch, M., Betts, A., and Scipal, K.: A revised hydrology for the ECMWF model: verification from field site to terrestrial water storage and impact in the Integrated Forecast System, Journal of Hydrometeorology, 10, 623–643, 2009.
- Barbu, A.-L., Calvet, J.-C., Demarty, J., Masson, V., and Mahfouf, J.-F.: Assimilation of Soil Wetness Index and Leaf Area Index into the ISBA-A-gs land surface model: grassland case study, Biogeosciences, 8, 1971–1986, https://doi.org/10.5194/bg-8-1971-2011, 2011.
- Baret, F., Weiss, M., Lacaze, R., Camacho, F., Makhmara, H., Pacholcyzk, P., and Smets, B.: GEOV1: LAI and FAPAR essential climate variables and FCOVER global time series capitalizing over existing products. Part1: Principles of development and production, Remote Sensing of Environment, 137, 299–309, https://doi.org/10.1016/j.rse.2012.12.027, 2013.
- Bonan, B. et al.: Machine learning for observation operators, Journal of Advances in Modeling Earth Systems, 15, e2022MS003 543, 2023.
- Boussetta, S. and Balsamo, G.: Vegetation dataset of Land Use/Land Cover and Leaf Area Index, https://confess-h2020.eu/wp-content/uploads/2021/08/confess-d1-1-v1-0-.pdf, deliverable D1.1, CONFESS Project, Horizon 2020, 2021.
- Boussetta, S., Balsamo, G., Arduini, G., Dutra, E., McNorton, J., Choulga, M., Agustí-Panareda, A., Beljaars, A., Wedi, N., Munõz-Sabater, J., de Rosnay, P., Sandu, I., Hadade, I., Carver, G., Mazzetti, C., Prudhomme, C., Yamazaki, D., and Zsoter, E.: ECLand: The ECMWF Land Surface Modelling System, Atmosphere, 2021.
- Burton, C., Lampe, S., Kelley, D. I., Thiery, W., Hantson, S., Christidis, N., Gudmundsson, L., Forrest, M., Burke, E., Chang, J., Huang, H., Ito, A., Kou-Giesbrecht, S., Lasslop, G., Li, W., Nieradzik, L., Li, F., Chen, Y., Randerson, J., Reyer, C. P. O., and Mengel, M.: Global burned area increasingly explained by climate change, Nature Climate Change, 14, 1186–1192, 2024.



- Calvet, J.-C., Bonan, B., Rojas-Munoz, O., Agustí-Panareda, A., de Rosnay, P., Weston, P., Peylin, P., Bacour, C., Bastrikov, V., Maignan, F., Kaminski, T., Knorr, W., Vossbeck, M., and Scholze, M.: Demonstrator ayatems for using remote sensing data (LAI, VOD, SIF) in online global prior fluxes for the CO2MVS prototype, Tech. Rep. D3.4, CoCO2 Consortium, 2023.
- Camps-Valls, G. et al.: Physics-aware machine learning for Earth system modelling, Nature Reviews Physics, 3, 422–440, 2021.
- Carmona-Moreno, C., Belward, A., Malingreau, J.-P., Hartley, A., Garcia-Alegre, M., Antonovskiy, M., Buchshtaber, V., and Pivovarov, V.: Characterizing interannual variations in global fire calendar using data from Earth observing satellites, Global Change Biology, 11, 2005.
- Courtier, P., Thépaut, J.-N., and Hollingsworth, A.: A strategy for operational implementation of 4D-Var, using an incremental approach, Quarterly Journal of the Royal Meteorological Society, https://doi.org/https://doi.org/10.1002/qj.49712051912, 1994.
- de Rosnay, P., Browne, P., de Boisséson, E., Fairbairn, D., Hirahara, Y., Ochi, K., Schepers, D., Weston, P., Zuo, H., Alonso-Balmaseda, M., Balsamo, G., Bonavita, M., Bormann, N., Brown, A., Chrust, M., Dahoui, M., De Chiara, G., English, S., Geer, A., Healy, S., Hersbach, H., Laloyaux, P., Magnusson, L., Massart, S., McNally, A., Pappenberger, F., and Rabier, F.: Coupled data assimilation at ECMWF: current status, challenges and future developments, Quarterly Journal of the Royal Meteorological Society, 148, 2672–2702, https://doi.org/10.1002/qj.4330, URL https://rmets.onlinelibrary.wiley.com/doi/abs/10.1002/qj.4330, 2022.
- Desroziers, G., Berre, L., Chapnik, B., and Poli, P.: Diagnosis of observation, background and analysis-error statistics in observation space, Quarterly Journal of the Royal Meteorological Society, 131, 3385–3396, https://doi.org/10.1256/qj.05.108, 2005.
- Di Giuseppe, F., Pappenberger, F., Wetterhall, F., Krzeminski, B., Camia, A., Libertá, G., and San Miguel, J.: The potential predictability of fire danger provided by numerical weather prediction, Journal of Applied Meteorology and Climatology, 55, 2469–2491, 2016.
- Di Giuseppe, F., Benedetti, A., Coughlan, R., Vitolo, C., and Vuckovic, M.: A Global Bottom-Up Approach to Estimate Fuel Consumed by Fires Using Above Ground Biomass Observations, Geophysical Research Letters, 48, e2021GL095 452, 2021.
- Di Giuseppe, F., McNorton, J., Lombardi, A., and Wetterhall, F.: Global data-driven prediction of fire activity, Nature Communications, 16, 2918, 2025.
- Dorigo, W. A., Gruber, A., De Jeu, R. A. M., Wagner, W., Stacke, T., Loew, A., Albergel, C., Brocca, L., Chung, D., Parinussa, R., Reichle, R., Rüdiger, C., Van Der Schalie, R., Vreugdenhil, M., and Zwieback, S.: The International Soil Moisture Network: serving Earth system science for over a decade, Hydrology and Earth System Sciences, 25, 5749–5804, https://doi.org/10.5194/hess-25-5749-2021, 2021.
- Drusch, M. and Viterbo, P.: Assimilation of Screen-Level Variables in ECMWF's Integrated Forecast System: A Study on the Impact on the Forecast Quality and Analyzed Soil Moisture, Monthly Weather Review, 135, 300–314, 2007.
- Drusch, M., Scipal, K., de Rosnay, P., Balsamo, G., Andersson, E., Bougeault, P., and Viterbo, P.: Towards a Kalman Filter based soil moisture analysis system for the operational ECMWF Integrated Forecast System, Geophysical Research Letters, 36, https://doi.org/10.1029/2009GL037716, 2009.



- El Garroussi, S., Di Giuseppe, F., Barnard, C., and Wetterhall, F.: Europe faces up to tenfold increase in extreme fires in a warming climate, npj Climate and Atmospheric Science, 7, 30, 2024.
- Fleming, L., Bean, J., Kirkpatrick, B., Cheng, Y., Pierce, R., Naar, J., Nierenberg, K., Backer, L., Wanner, A., Reich, A., Zhou, Y., Watkins, S., Henry, M., Zaias, J., Abraham, W., Benson, J., Cassedy, A., Hollenbeck, J., Kirkpatrick, G., Clarke, T., and Baden, D.: Exposure and effect assessment of aerosolized red tide toxins (brevetoxins) and asthma., Environmental Health Perspectives, https://doi.org/https://doi.org/10.17226/13115, 2009.
- Fuster, B., Sánchez-Zapero, J., Camacho de Coca, F., Garcia-Santos, V., Verger, A., Lacaze, R., Weiss, M., Frederic, B., and Smets, B.: Quality Assessment of PROBA-V LAI, fAPAR and fCOVER Collection 300 m Products of Copernicus Global Land Service, Remote Sensing, 12, 2020.
- Garrigues, S., de Rosnay, P., Weston, P., Fairbain, D., Pinnington, E., Agusti-Panareda, A., Boussetta, S., Calvet, J., Bacour, C., and Engelen, R.: Assimilation of solar induced chlorophyll fluorescence satellite observations in the ECMWF Integrated Forecast System, QJRS, 2025.
- Guanter, L., Bacour, C., Schneider, A., Aben, I., van Kempen, T. A., Maignan, F., Retscher, C., Köhler, P., Frankenberg, C., Joiner, J., and Zhang, Y.: The TROPOSIF global sun-induced fluorescence dataset from the Sentinel-5P TROPOMI mission, Earth System Science Data, 13, 5423–5440, 2021.
- Hantson, S., Andela, N., Goulden, M. L., and Randerson, J. T.: Human-ignited fires result in more extreme fire behavior and ecosystem impacts, Nature Communications, 13, 2022.
- Hood, S. M., Varner, J. M., Jain, T. B., and Kane, J. M.: A framework for quantifying forest wildfire hazard and fuel treatment effectiveness from stands to landscapes, Fire Ecology, 18, 2022.
- Ivison, K., Little, K., Orpin, A., Kettridge, N., and Davies, G. M.: A national-scale sampled temperate fuel moisture database, Scientific Data, 11, 973, https://doi.org/10.1038/s41597-024-03832-w, 2024.
- Ivison, K., Little, K., Belcher, C. M., Crawford, A. J., Davidson, S. J., Graham, L. J., and Kettridge, N.: Citizen science as a tool to investigate landscape controls on fuel moisture and flammability, Journal of Pyrogeography, https://doi.org/https://doi.org/10.1016/j.pyro.2025.100002, 2025.
- Jacquemoud, S. and Baret, F.: PROSPECT: A model of leaf optical properties spectra, Remote Sensing of Environment, 34, 75–91, 1990.
- K. Scipal, M. Drusch, and W. Wagner: Assimilation of a ERS scatterometer derived soil moisture index in the ECMWF numerical weather prediction system, Advances in water resources, https://doi.org/ https://doi.org/10.1016/j.advwatres.2008.04.013, 2008.
- Kumar, S. V., Mocko, D. M., Wang, S., Peters-Lidard, C. D., and Borak, J.: Assimilation of Remotely Sensed Leaf Area Index into the Noah-MP Land Surface Model: Impacts on Water and Carbon Fluxes and States over the Continental United States, Journal of Hydrometeorology, 20, 1359 1377, https://doi.org/10.1175/JHM-D-18-0237.1, 2019.
- Little, K., Graham, L. J., and Kettridge, N.: Accounting for among-sampler variability improves confidence in fuel moisture content field measurements, International Journal of Wildland Fire, 33, 1–13, https://doi.org/10.1071/WF23078, 2024.
- McNorton, J. R. and Di Giuseppe, F.: A global fuel characteristic model and dataset for wildfire prediction, Biogeosciences, https://doi.org/https://doi.org/10.5194/bg-21-279-2024, 2024.



- McNorton, J. R., Di Giuseppe, F., Pinnington, E., Chantry, M., and Barnard, C.: A Global Probability-Of-Fire (PoF) Forecast, Geophysical Research Letters, 51, https://doi.org/https://doi.org/10.1029/2023GL107929, 2024.
- Muñoz Sabater, J., Dutra, E., Agustí-Panareda, A., Albergel, C., Arduini, G., Balsamo, G., Boussetta, S., Choulga, M., Harrigan, S., Hersbach, H., Martens, B., Miralles, D. G., Piles, M., Rodríguez-Fernández, N. J., Zsoter, E., Buontempo, C., and Thépaut, J.-N.: ERA5-Land: a state-of-the-art global reanalysis dataset for land applications, Earth System Science Data, 13, 4349–4383, 2021.
- Muñoz-Sabater, J., Dutra, E., Agustí-Panareda, A., Albergel, C., Arduini, G., Balsamo, G., Boussetta, S., Choulga, M., Harrigan, S., Hersbach, H., Martens, B., Miralles, D. G., Piles, M., Rodríguez-Fernández, N. J., Zsoter, E., Buontempo, C., and Thépaut, J.-N.: ERA5-Land: a state-of-the-art global reanalysis dataset for land applications, Earth System Science Data, 13, 4349–4383, https://doi.org/10.5194/essd-13-4349-2021, 2021.
- Reichle, R. and Koster, R.: Bias reduction in short records of satellite soil moisture, Geophysical Research Letters, 31, L19 501, 2004.
- Reichstein, M. et al.: Deep learning and process understanding for data-driven Earth system science, Nature, 566, 195–204, 2019.
- Rodríguez-Fernández, N. J., Mialon, A., Mermoz, S., Bouvet, A., Richaume, P., Al Bitar, A., Al-Yaari, A., Brandt, M., Kaminski, T., Le Toan, T., Kerr, Y. H., and Wigneron, J.-P.: An evaluation of SMOS Lband vegetation optical depth (L-VOD) data sets: high sensitivity of L-VOD to above-ground biomass in Africa, Biogeosciences, 15, 4627–4645, 2018.
- Rosnay, P., Drusch, M., Vasiljevic, D., Balsamo, G., Albergel, C., and Isaksen, L.: A simplified Extended Kalman Filter for the global operational soil moisture analysis at ECMWF, Quarterly Journal of the Royal Meteorological Society, 139, 2013.
- Sabater, J. M., Rüdiger, C., Calvet, J.-C., Fritz, N., Jarlan, L., and Kerr, Y.: Joint assimilation of surface soil moisture and LAI observations into a land surface model, Agricultural and Forest Meteorology, 148, 1362–1373, https://doi.org/10.1016/j.agrformet.2008.04.003, 2008.
- Ulaby, F. T., Moore, R. K., and Fung, A. K.: Microwave remote sensing: Active and passive. volume 1-microwave remote sensing fundamentals and radiometry, Earth Resources And Remote Sensing, NASA, 1981.
- Verger, A., Weiss, M., Baret, F., Camacho, F., and Makhmara, H.: Leaf Area Index 2014-present (raster 300 m), global, 10-daily version 1, Copernicus Global Land Service, https://doi.org/10. 2909/219fdc9f-616b-444b-a495-198f527b4722, URL https://land.copernicus.eu/en/products/vegetation/leaf-area-index-300m-v1.0, 2019.
- Verhoef, W.: Light scattering by leaf layers with application to canopy reflectance modeling, Remote Sensing of Environment, 16, 125–141, 1984.
- Wagner, W., Hahn, S., Kidd, R., Melzer, T., Bartalis, Z., Hasenauer, S., Figa-saldaña, J., Rosnay, P., Jann, A., Schneider, S., Komma, J., Kubu, G., Brugger, K., Aubrecht, C., Züger, J., Gangkofner, U., Kienberger, S., Brocca, L., Wang, Y., and Rubel, F.: The ASCAT Soil Moisture Product: A Review of its Specifications, Validation Results, and Emerging Applications, Meteorologische Zeitschrift, 2013.
- Widlowski, J.-L. et al.: The fourth phase of the Radiation Transfer Model Intercomparison (RAMI) exercise, Journal of Geophysical Research: Atmospheres, 120, 9401–9423, 2015.



Yebra, M., Scortechini, G., Adeline, K., Aktepe, N., Almoustafa, T., Bar-Massada, A., Beget, M. E., Boer, M., Bradstock, R., Brown, T., Castro, F. X., Chen, R., Chuvieco, E., Danson, M., Degirmenci, C. U., Delgado-Dávila, R., Dennison, P., Di Bella, C., Domenech, O., Féret, J.-B., Forsyth, G., Gabriel, E., Gagkas, Z., Gharbi, F., Granda, E., Griebel, A., He, B., Jolly, M., Kotzur, I., Kraaij, T., Kristina, A., Kütküt, P., Limousin, J.-M., Martín, M. P., Monteiro, A. T., Morais, M., Moreira, B., Mouillot, F., Msweli, S., Nolan, R. H., Pellizzaro, G., Qi, Y., Quan, X., Resco de Dios, V., Roberts, D., Tavşanoğlu, c., Taylor, A. F. S., Taylor, J., Tüfekçioğlu, I., Ventura, A., and Younes Cardenas, N.: Globe-LFMC 2.0, an enhanced and updated dataset for live fuel moisture content research, Scientific Data, 11, 332, 2024.